A Monomeric Human Apolipoprotein E Carboxyl-Terminal Domain†

Daping Fan,‡ Qianqian Li,§ Leslie Korando,‡ W. Gray Jerome,|| and Jianjun Wang*,‡

Department of Biochemistry and Molecular Biology and Department of Anatomy, School of Medicine, Southern Illinois University at Carbondale, Carbondale, Illinois 62901-4413, and Department of Pathology, Vanderbilt University Medical Center, B-2101 MCN, 1161 21st Avenue South, Nashville, Tennessee 37232-2561

Received November 3, 2003; Revised Manuscript Received February 19, 2004

ABSTRACT: ApoE plays a critical role in lipoprotein metabolism and plasma lipid homeostasis through its high-affinity binding to the LDL-receptor family. In solution, apoE is an oligomeric protein and the C-terminal domain causes apoE's aggregation. The aggregation property presents a major difficulty for the structural determination of this protein. A high-level expression system of the apoE C-terminal domain is reported here. Using protein engineering techniques, we identified a monomeric, biologically active apoE C-terminal domain mutant. This mutant replaces five bulky hydrophobic residues in the region of residues 253−289 with either smaller hydrophobic or polar/charged residues (F257A, W264R, V269A, L279Q, and V287E). The solubility of the mutant is significantly increased (∼10-fold). Cross-linking experiments indicate that this mutant is 100% monomeric even at 5 mg/mL. CD and guanidine hydrochloride denaturation results indicate that the mutant maintains an identical α-helical secondary structure and stability as compared with those of the wild-type protein. DMPC-binding assays demonstrate an identical vesicle clearance rate shared by both the mutant and the wild-type apoE C-terminal domain. In addition, electron microscopic results show identical recombinant HDL particles prepared with both the mutant and the wild-type proteins. These results indicate that residues F257, W264, V269, L279, and V287 are critical residues for aggregation but may not be important in maintaining the structure, stability, and lipid-binding activity of this apoE domain, suggesting that apoE may use different "epitopes" for its aggregation property, helical structure/stability, and lipid-binding activity. Finally, preliminary NMR data demonstrated that we have collected high-quality NMR spectra, allowing for an NMR structural determination of the apoE C-terminal domain.

Human apoE[1] is a 299-residue, 34 kDa exchangeable apolipoprotein, which plays a central role in the regulation of lipid metabolism through its high-affinity interaction with cell surface receptors, including the LDL receptor and LRP (*1*). Defective binding of apoE to the LDL receptor results in the accumulation of cholesterol-rich lipoprotein particles in plasma, leading to the formation of atherosclerotic plaques and ultimately causing coronary artery disease (*1*, *2*). Three major isoforms of apoE have been identified: ApoE3 has a cysteine at position 112 and an arginine at position 158, while apoE2 has cysteines and apoE4 has arginines at both positions (*3*, *4*). The most common isoform, apoE3, binds to the LDL receptor (100% affinity) and regulates a normal lipoprotein metabolism. ApoE2, on the other hand, binds to the LDL receptor defectively (∼2% affinity) and is associated with type III hyperlipoproteinemia (*5*). ApoE4 is associated with a high risk of heart disease (*6*) and is one of the major genetic risk factors for Alzheimer's disease (*7*).

ApoE is a two-domain protein that contains a 22 kDa N-terminal domain (residues 1−191) and a 10 kDa C-terminal domain (residues 216−299), linked by a protease-sensitive hinge region (*1*, *8*). Experimental data indicates that these two domains fold relatively independent of one another and have distinct functions. While the N-terminal domain is mainly responsible for the LDL-receptor binding, the C-terminal domain binds to lipoprotein with a high affinity (*1*, *9*). Interestingly, the apoE N-terminal domain also strongly binds to heparin but only displays a weak lipid-binding activity (*1*). Controversial results have been published for the apoE−Aβ4 interactions, suggesting that both domains of apoE bind to Aβ4, with a stronger binding activity of the C-terminal domain (*10*, *11*). Experimental data indicated that apoE forms oligomers and the C-terminal domain is responsible for oligomerization (*1*). The aggregation property and the intrinsic flexibility of the C-terminal domain make the structural determinations of the C-terminal domain and full-length apoE unsuccessful. Efforts in the structural determination of the apoE C-terminal domain and full-length apoE have yielded diffraction quality crystals of a 50-residue

† This work was supported by a Scientist Development Grant from the American Heart Association, Midwest Affiliate, Inc. (AHA 0130546Z to J.W.), and RO1 grants from the NIH (HL074365 to J.W. and HL49148 to W.G.J.). D.F. is supported by predoctoral fellowships from the American Heart Association (AHA 0110244Z and AHA0315270Z).

* To whom correspondence should be addressed. E-mail: jwang@siumed.edu. Tel: 618-453-5002. Fax: 618-453-6440.

‡ Department of Biochemistry and Molecular Biology, Southern Illinois University at Carbondale.

§ Department of Anatomy, Southern Illinois University at Carbondale.

|| Vanderbilt University Medical Center.

[1] Abbreviations: apoE, apolipoprotein E; apoEC, the apoE C-terminal domain; apoEC-J, the monomeric, biologically active apoE C-terminal domain mutant; apoEC-WT, the wild-type apoE C-terminal domain; DMPC, dimyristoylphosphatidylcholine; DPC, dodecylphosphocholine; IPTG, isopropyl β-D-thiogalactoside; LDL, low-density lipoprotein; LDLR, low-density lipoprotein receptor; LRP, LDL-receptor-related protein; NMR, nuclear magnetic resonance; CD, circular dichroism.

10.1021/bi035958w CCC: $27.50
Published on Web 04/07/2004

fragment of the C-terminal domain (*12*). However, no detailed structural information is available for either the full-length apoE or its C-terminal domain to date.

The N-terminal domain of apoE is monomeric. The X-ray crystal structure of this domain in the lipid-free state reveals a globular up-and-down bundle of four amphipathic α-helices that sequester their hydrophobic faces from aqueous solution, while the hydrophilic surfaces of the bundle point to the solvent (*13*). The LDL-receptor binding region, residues 130−150, is located at helix 4 that is exposed to the solvent. Experimental data demonstrated that both full-length apoE and the apoE N-terminal domain display a minimum LDL-receptor binding activity in the absence of lipid. However, upon binding to lipid, the LDL-receptor binding activity is fully recovered (*14*, *15*). This indicates that the lipid-binding activity of apoE is critical for the expression of its receptor binding activity. Since the C-terminal domain of apoE is responsible for high-affinity lipid binding, structures of this domain in both the lipid-free and lipid-bound states are essential for us in understanding how the lipid-binding activity induces a competent conformation for apoE's LDL-receptor binding activity, and currently we do not have such structures available.

A domain−domain interaction is observed in apoE that seems to regulate its biological functions. One example is that an isoform-specific difference in the apoE N-terminal domain modulates the lipoprotein-binding preferences elicited by the C-terminal domain (*16*). Using crystallographic study and site-directed mutagenesis, Weisgraber's group showed that a substitution of C112 by an arginine in the N-terminal domain (apoE3 → apoE4) moved the side chain of R61 away from its usual position, potentially resulting in the formation of a salt bridge with E255 in the C-terminal domain (*17*−*19*). It is hypothesized that this new salt bridge between the two domains may change the overall conformation of apoE4, resulting in the VLDL binding preference of apoE4, while apoE2 and apoE3 preferably bind to HDL (*18*). A final verification of this hypothesis requires a structure of full-length apoE4. In addition, a change in the C-terminal domain also modulates apoE's receptor binding activity displayed by the N-terminal domain (*20*, *21*). The structural basis for this functional modulation by apoE isoforms is also unknown.

We are interested in structural studies of apoE using NMR techniques. To carry out an NMR structural determination, we have to solve the aggregation problem of this protein. Since the C-terminal domain causes apoE's aggregation, we focused our attention on this domain. We suggest that the apoE C-terminal domain uses different "epitopes" to regulate its lipid-binding activity, to maintain and stabilize its α-helical structure, and to mediate its aggregation. This hypothesis is based on previously published work by Weisgraber's group, indicating that residues 268−289 are responsible for apoE's tetramerization, whereas residues 225−272 are critical for lipoprotein binding (*22*). Using protein engineering techniques, we carefully designed and prepared a series of mutants of the apoE C-terminal domain (spanning residues 200−299) with the aim of preparing a monomeric, biologically active apoE C-terminal domain. We report here that we identified an apoE C-terminal domain mutant (apoEC-J) that is monomeric at 5 mg/mL. The secondary structure and stability of this monomeric mutant are essentially identical to the wild-type apoEC (apoEC-WT). More importantly, apoEC-J also displays a lipid-binding activity identical to that of the apoEC-WT. With this monomeric, biologically active apoE C-terminal domain mutant, we demonstrate that we have collected high-quality NMR spectra for the structural determination of the apoE C-terminal domain in both the lipid-free and lipid-bound states.

EXPERIMENTAL PROCEDURES

High-Level Expression of the ApoE C-Terminal Domain. *Eco*RI and *Hin*dIII sites were used for subcloning the apoEC (residues 200−299) into an engineered pET30a(+) plasmid vector (Novagen), in which the large His tag (6 kDa) was replaced by a fragment of six consecutive His residues with two linker Ser residues, followed by a factor Xa cleavage site. With this DNA construct, expression was carried out using *Escherichia coli* BL-21(DE3) cells. Briefly, minimum medium (kanamycin, 30 mg/L) was used for the cell culture which was grown at 37 °C until it reached an OD at 600 nm of 0.8−1.0. Expression was then induced by IPTG (0.25 mM final concentration) and continued overnight at 20 °C. The cells were harvested by centrifugation. The cell pellet was resuspended in 10 mL/g cells with binding buffer (20 mM Tris-HCl, 500 mM NaCl, 2.5 mM imidazole, and 0.1 mM PMSF at pH 7.9) and then sonicated on ice. Bacterial debris was removed by centrifugation. The pellet was redissolved in 6−8 M urea and sonicated. All supernatant fractions were combined and applied on a His·Bind resin column (Novagen). The column was washed with binding buffer and then wash buffer containing 50 mM imidazole. The purified recombinant protein was eluted from the column using a buffer containing 1.0 M imidazole. The eluted protein was dialyzed against 50 mM ammonium bicarbonate to remove imidazole and then lyophilized. Factor Xa cleavage was carried out at an enzyme/protein ratio of 1:200 at 2−4 °C for 24 h at 1 mg/mL protein concentration in factor Xa cleavage buffer (50 mM Tris-HCl, pH 8.0, 0.1 M NaCl, and 5 mM $CaCl_2$) with slight shaking. The reaction products were subjected to the factor Xa resin (Novagen) to remove factor Xa and then reloaded onto the His·Bind resin column to remove the His tag. The purified protein was then dialyzed against 50 mM ammonium bicarbonate and lyophilized. Using this expression system, we can routinely produce ∼50 mg/L purified apoEC-WT and its mutants.

Site-Directed Mutagenesis. Site-directed mutagenesis was carried out using the QuickChange mutagenesis kit from Stratagene (Stratagene, La Jolla, CA). Briefly, primers containing the desired mutations were annealed to the denatured DNA expression vector harboring the apoEC-WT gene, which was then extended using PfuTurbo DNA polymerase to generate nicked, circular strands. The methylated, nonmutated parental DNA was digested using *Dpn*I. The circular, nicked, double-stranded DNA containing the mutation was then transformed into *E. coli* cells. The mutations were confirmed by DNA sequencing.

Cross-Linking Experiments. Lipid-free apoEC-WT and apoEC-J in 20 mM phosphate buffer, different NaCl concentrations, and different pHs were incubated for 30 min with bis(sulfosuccinmidyl) suberate (BS_3; Pierce, final concentration 0.5 mM). The cross-linking reaction mixture was quenched by adding 1 M Tris-HCl and 5 × SDS−PAGE

sample buffer and then loaded on a 6−15% SDS−PAGE gel.

Dimyristoylphosphatidylcholine (DMPC) Binding Assay. Ten milligrams of DMPC (Avanti Polar Lipids Inc., Alabaster, AL) was dissolved in a mixture of chloroform and methanol (3:1 v/v), dried using N_2, and placed under a vacuum for at least 10 h. One milliliter of prewarmed buffer was added (20 mM Tris-HCl, pH 7.2, 250 mM NaCl, and 1 mM EDTA) to a final lipid concentration of 10 mg/mL, and the mixture was vortexed several times for 30 s each. Using a 200 nm filter, unilamellar vesicles (∼200 nm in diameter) were prepared by extrusion (*23*). The protein-induced transformation of DMPC vesicles into protein/DMPC discoidal complexes was monitored as a function of time (*24*). Vesicles (250 μg) and 150 μg of apoEC in buffer were added into a thermostated 1 mL cuvette and mixed for 5−10 s at 24 °C, and clearance of the solution was monitored using a Perkin-Elmer spectrophotometer (model Lambda 3B) at 490 nm. All solutions were preincubated at 24 °C before the reaction.

Preparation of Reconstituted HDL. The rHDL particles were prepared using the sodium cholate dialysis method (*25*−*26*) with POPC, cholesterol, apoEC, and sodium cholate in a molar ratio of 80:8:1:80. The mixture of POPC and cholesterol was dissolved in $CHCl_3$, dried under nitrogen, and then resuspended in Tris−saline buffer (10 mM Tris, 0.15 M NaCl, 1 mM NaN_3, and 0.01% EDTA, pH 8.0). After being vortexed thoroughly, sodium cholate was added into the mixture, and the mixture was then vortexed again for another 3 min. The dispersion was incubated at 37 °C and vortexed every 15 min until completely clear. ApoEC protein was added, and the mixture was incubated for 1 h at 37 °C. Sodium cholate was removed by exhaustive dialysis.

Electron Microscopy. The rHDL and DMPC particles were adsorbed to hydrophilic, carbon and Formvar-coated grids. Samples were negatively stained for 20 s with 2% phosphotungstic acid, pH 7.0. Digital images were taken using a Philips CM-30 electron microscope equipped at 80 keV accelerating voltage. For quantification, at least 10 arbitrarily selected fields were chosen, and the largest diameter of each particle was measured (>250 particles per condition).

Circular Dichroism Spectroscopy and Protein Stability Measurement. Circular dichroism (CD) measurements were carried out on an AVIV Model 62DS CD spectrometer (AVIV Instruments, Inc., Lakewood, NJ) with a variable temperature capability under computer control within ±0.2 °C. For the chemical denaturation experiments, data were collected at a single wavelength for 60 s. Guanidine hydrochloride denaturation was performed as described (*27*) and monitored by CD at 220 nm in a 0.1 cm path length cuvette. Individual 0.4 mL samples were prepared by weight for each denaturant concentration. The concentrations of protein and denaturant were determined using the density formulas given by Pace et al. (*27*).

NMR Methods. The NMR sample contained 1 mM ^{15}N-labeled protein in 65% H_2O/5% D_2O/30% TFE-d_3, 200 mM phosphate buffer (pH 5.7), and 1 mM NaN_3 or 95% H_2O/5% D_2O with 150 mM DPC-d_{38}. The chemical shift was referenced using DSS (2,2-dimethyl-2-silapentane-5-sulfonate) at 0 ppm. All NMR experiments were performed at 30 °C on a Varian Inova 500 spectrometer equipped with a triple-resonance, *z*-axis gradient probe. The 2D ^{1}H−^{15}N HSQC collected was a sensitivity-enhanced experiment with 1024 points at the proton dimension and 256 complex points at the ^{15}N dimension. The acquisition times for both dimensions were 64 ms. The NMR data processing was achieved using nmrPipe and nmrDraw software (*28*) and analyzed with PIPP (*29*).

RESULTS

High-Level Expression of the ApoE C-Terminal Domain. Using our expression system, we can routinely produce 50 mg/L purified apoEC-WT. Since we used an engineered pET30a(+) expression vector, the expressed apoEC-WT only contains six His plus a two Ser linker. To remove the His tag, we also introduced a factor Xa site between the His tag and apoEC. Thus, the expressed protein contains 12 extra residues in addition to apoEC. We found that the factor Xa digestion has to be carried out at a lower temperature, typically 2−4 °C. The mass spectrum shows the correct molecular weight of apoEC-WT and apoEC-J.

Factors That May Cause ApoE Aggregation. Figure 1 shows the sequence alignment of the apoE C-terminal domain (residues 200−299) across nine different species. This alignment demonstrates that a fragment of residues 253−289 is the most conserved region, indicating the potential functional/structural importance. We suggest that this region may also be responsible for apoE's aggregation. This is supported by previous published results. For example, Aggerbeck et al. demonstrated that the apoE C-terminal domain is tetrameric, while the N-terminal domain is monomeric (*9*). Using several apoE C-terminal truncation mutants, Weisgraber's group further suggested that residues 268−289 were responsible for apoE's aggregation and residues 225−272 were critical for its lipoprotein-binding activity (*17*, *22*). Secondary structure predictions suggested that residues 225−266 are a class A helix (**T**$_{225}$RDR**L**DE-**V**KEQ**VA**E**V**R**A**K**L**EEQ**A**QQ**I**R**L**Q**A**E**AF**Q**A**R**L**KS**WF**-E$_{266}$), which is a lipid-binding helix, and residues 267−289 are a class G* helix (**P**$_{267}$**LV**ED**M**QRQ**WA**G**LV**EK**V**Q**AAV**-G**T**$_{289}$), which is a helix in globular proteins (the bold residues are hydrophobic residues) (*30*). In fact, the N-terminal half of residues 225−266 is a standard class A helix with hydrophobic residues every two to three residues apart, but the C-terminal half of residues 225−266 is more similar to a class G* helix with more bulky hydrophobic residues along its sequence. In the class G* helix, more hydrophobic residues are observed, especially several consecutive, bulky (β-branched) hydrophobic residues. We suggest that a high density of consecutive bulky hydrophobic residues, such as Val, Leu, Trp, and Phe, in this region is the main reason for apoE's aggregation. Indeed, many consecutive bulky hydrophobic residues are found in residues 253−289, such as WF, PLV, and LV. In contrast, hydrophobic residues are evenly distributed in the rest of the regions of this apoE domain, typically every two to three residues apart. These consecutive, bulky hydrophobic residues form large cross-sectional, hydrophobic layers in the helix, resulting in apoE aggregation (Figure 2, left).

Rationale for Preparing a Monomeric, Biologically Active ApoE C-Terminal Domain. Using molecular modeling, a model tetramer was prepared that mimics tetramerization of apoE, as shown in Figure 2. In the left panel, one of the

```
apoE  human GQPLQERAQAWGERLRARMEEMGSRTRDRLDEVKEQVAEVRAKLEEQAQQ    249
apoE baboon SQPLQERAQALGERLRARMEEMGSRTRDRLDEVKEQVAEVRAKLEEQAQQ    249
apoE bovine GQPLLERAEAWRQKLHGRLEEVGVRAQDRLDKIRQQLEEVHAKVEEQGNQ    249
apoE  pig   GQPLRERAEAWGQKLRGRLEEMGSRTRDRLDEMRDELEEVRTKVEEQGSQ    249
apoE rabbit GRPLRERAQAWGERLRGHLEEVGSRARDRLNEVREQVEEVRVKVEEQAPQ    249
apoE  rat   PAP RDRAQALSDRIRGRLEEVGNQARDRLEEVREQMEEVRSKMEEQTQQ    248
apoE  mouse AQPLRDRAQAFGDRIRGRLEEVGNQARDRLEEVREHMEEVRSKMEEQTQQ    249
apoE  gpig  SQPLQERAQAWGEQMRGRLEKVGSQARDRLEEVREQMEEVRVKVEEQ      246
apoE monkey SQPLQERAQALGERLRARMEEMGSRTRDRLDEVKEQVAEVRAKLEEQAQQ    249
   Summary: --PL-ERAQA*-*R*R-R*EE-G---*DRL*E***-*-EV*-K*EEQ--Q
                 |<---Class A Helix--->|  |<------ Class A
                253                                289
apoE  human IRLQAEAFQARLKSWFEPLVEDMQRQWAGLVEKVQAAVG TSAAP   VPSDNH    299
apoE baboon ISLQAEAFQARLKSWFEPLVEDMQRQWAGLVEKVQAAVG ASTAP   VPSDNH    299
apoE bovine MRLQAEAFQARLRSWFEPLVEDMQRQWAGLVEKVQLALR PSPTS   PPSENH    299
apoE  pig   LRLQAEAFQARLKGWFEPLVEDMRRQWAGLVERMQSAVSISSSTS   APSDNQ    300
apoE rabbit MRLQAEAFQARLKSWFEPLVEDMQRQWAGLVEKLQAAMPSKAPAA   APIENQ    300
apoE  rat   IRLQAEIFQARIKGWFEPLVEDMQRQWANLMEKIQASVATNSIASTT VPLENQ    301
apoE  mouse IRLQAEIFQARLKGWFEPIVEDMHRQWANLMEKIQASVATNPII TP VAQENQ    301
apoE  gpig    AEAFQARLKSWFEPMMEDMRRQWAELIQKVQVAVG   ASTS APSQEP    291
apoE monkey ISLQAEAFQARLKSWFEPLVEDMQRQWAGLVEKVQAAVG ASTAP   VPIDNH    299
   Summary: --LQAE*FQARLK*WFEP*VEDM-RQWA-L*EK*QAAV*---------P--N-
               Helix------>|  |<---Class G* Helix--->
```

FIGURE 1: Sequence alignment of the apoE C-terminal domain (residues 200−299) across nine different species. The predicted secondary structure is listed at the bottom of the sequence. The most conserved region is highlighted in the dotted line box.

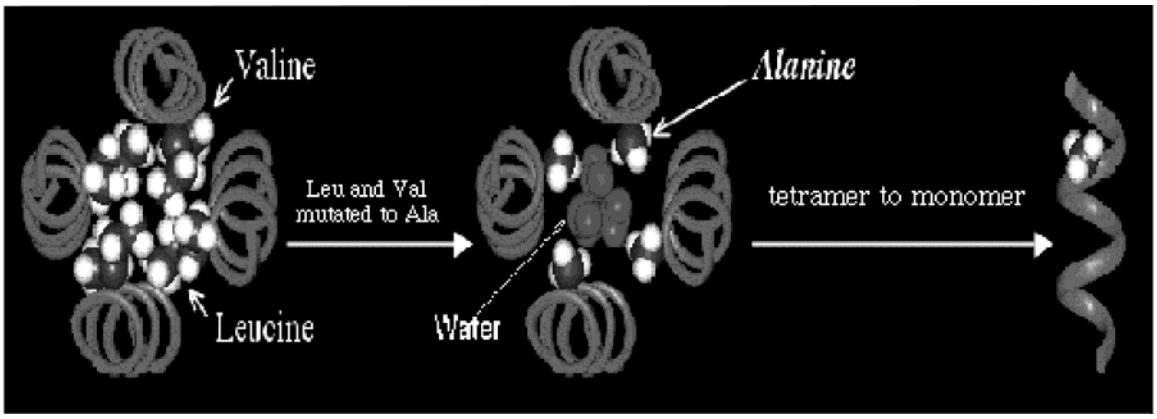

FIGURE 2: Model tetramer structure of the G* helices mimicking the tetramerization of apoE. Left panel: one of the large hydrophobic cross sections formed by the LV residues. Middle panel: Leu and Val are replaced by an Ala residue, and a water molecule is able to penetrate into the hydrophobic core of the tetramer. Right panel: the tetramer becomes monomers.

large hydrophobic layers formed by the LV residues was shown, demonstrating the hydrophobic−hydrophobic interactions in the apoE tetramer. The bulky hydrophobic residues form a large hydrophobic core in the bundle, stabilizing the tetrameric apoE structure. Replacing these bulky hydrophobic residues by either smaller side-chain residues, such as Ala, or polar residues, such as Gln or Asn, will significantly reduce the hydrophobic−hydrophobic interactions in the tetramer. As a consequence, the tetramer interior may be accessible by water molecules, as shown in the middle panel. Water molecules in the interior may break up the tetrameric helix−bundle into a monomeric helix (right panel), thus producing a monomeric apoE C-terminal domain.

A Monomeric, Biologically Active ApoE C-Terminal Domain. Following the above rationale, we initially designed several mutants. Our attention was focused on the region of residues 253−289, since previously published data indicated that residues 225−272 are responsible for apoE's lipoprotein-binding activity, whereas residues 267−289 are responsible for its tetramerization (*17*, *22*). For the first step, single amino acid mutations were generated on residues F257, W264, L268, V269, W276, L279, V280, and V287. Double mutants were then prepared and tested for their oligomeric states. Experimental results from the double mutants provide a guide for us to design multiple-site mutants, including three, four, and five amino acids. Using such an iterative procedure, a total of 13 multiple-site mutants in the region of residues 253−287 were prepared. Table 1 lists these multiple-site mutants with their mutation sites and replaced amino acids.

Using cross-linking experiments, the oligomeric states of the mutants at NMR concentrations (∼0.5−1.0 mM) were characterized. Our strategy was to first quickly identify a monomeric mutant and, then carry out careful experiments to characterize this mutant in terms of its structure and functions. Using this strategy, a monomeric mutant, apoEC-J, was quickly identified. Figure 3, panel A, shows an SDS−PAGE of the cross-linking results of apoEC-J, one single mutant, apoEC-W264R, and apoEC-WT as the control, demonstrating that apoEC-J is monomeric at 2 mg/mL, whereas both apoEC-W264R and apoEC-WT form a mixture of monomer, dimer, trimer, and tetramer at 1 mg/mL. Indeed, cross-linking experiments of apoEC-J at 5 mg/mL also show

Table 1: List of the Multiple-Site Mutants of the ApoE C-Terminal Domain

ID	F257A	W264R	L268Q	V269A	W276A	L279Q	V280A	V287E
apoEC-W264R		+						
apoEC-269		+		+				
apoEC-280		+					+	
apoEC-A		+		+			+	
apoEC-B		+					+	+
apoEC-C			+				+	
apoEC-D		+				+	+	
apoEC-E	+	+		+			+	
apoEC-F	+		+				+	
apoEC-G	+	+					+	
apoEC-H	+				+			+
apoEC-I	+		+		+			
apoEC-J	+	+		+		+		+
apoEC-K		+		+			+	+

that apoEC-J is monomeric. Figure 3, panels B and C, shows the SDS−PAGE of the cross-linking results of apoEC-J and apoEC-WT under different salt concentrations and different pHs, indicating that apoEC-J is always monomeric under all the conditions at 5 mg/mL, whereas apoEC-WT forms different oligomers under these conditions at 1 mg/mL. Interestingly, the solubility of apoEC-J is also significantly increased. The solubility of apoEC-WT is about 1.5 mg/mL (∼0.1 mM) in phosphate buffer; however, up to 10 mg/mL of apoEC-J can be dissolved (∼1 mM). Such an improvement in solubility of apoEC-J certainly facilitates structural studies of this protein.

Once monomeric apoEC-J was identified, we carried out a careful characterization of this mutant for its biophysical properties, such as structure, stability, and biological activity, since our goal was to obtain a monomeric apoE C-terminal domain that was biologically active. Using CD spectroscopy, the secondary structures of apoEC-J, apoEC-W264R, and apoEC-WT were compared. Figure 4, panel A, indicates that both apoEC-J and apoEC-W264R adopt a secondary structure identical to that of apoEC-WT. We then carried out GdnHCl denaturation experiments of the two apoEC mutants and apoEC-WT using CD spectroscopy. Our result also indicates that all three proteins share an identical stability (Figure 4, panel B). The GdnHCl half, $[GdnHCl]_{1/2}$, is ∼0.8 M for all three proteins, with the $\Delta G_D^{H_2O}$ for apoEC-WT, 3.78 kcal/mol, for apoEC-J, 3.50 kcal/mol, and for apoEC-W264R, 3.72 kcal/mol. These results are very similar to the published data which ranged between 3.8 and 4.0 kcal/mol for apoE-(216−299) (*8*). Thus, we conclude that the mutations in apoEC-J do not change the secondary structure and thermodynamic stability of the apoE C-terminal domain.

To examine the biological function of apoEC-J, two lipid-binding assays were performed. Since the primary biological function of the apoE C-terminal domain is the lipoprotein-binding activity, monomeric apoEC-J is considered to be biologically active only if it displays a lipid-binding activity equal to that of apoEC-WT. A DMPC binding assay was first used. This assay utilizes the lipid-binding activity of the apoE C-terminal domain, which spontaneously transforms larger DMPC vesicles into smaller discoidal apoEC/DMPC complexes. Figure 5 shows the result of the DMPC-binding assay of apoEC-J, apoEC-W264R, and apoEC-WT with a control of no protein added. Our results clearly demonstrate that incubation of DMPC vesicles without protein results in sample turbidity as monitored by OD measurements at 490 nm. However, this turbidity can be cleared if the DMPC vesicles are incubated with apoEC-WT, since apoEC-WT binds to the DMPC vesicles to form disklike particles. Incubations of DMPC vesicles with either apoEC-J or apoEC-W264R display a result identical to that of apoEC-WT. The phospholipid-binding kinetics is difficult to estimate accurately, since the binding interaction between apoEC-J/apoEC-WT and DPMC is very fast with a $t_{1/2}$ of <1 min. This result indicates that the monomeric mutant, apoEC-J, displays a DMPC vesicle clearance rate equal to that of apoEC-WT. Interestingly, the turbidity clearance by apoEC-J also displays an identical initial rate, suggesting an identical kinetics of DMPC clearance by both apoEC-WT and monomeric apoEC-J. Figure 6, lower panels, show the electron microscopic images of the discoidal particles generated by DMPC and apoEC-J or apoEC-WT. Electron microscopy confirmed that many of the particles formed were disks with a diameter of ∼18 nm. Moreover, it is clear that identical discoidal particles were formed during DMPC clearance assay using both apoEC-J and apoEC-WT. Second, we prepared recombinant HDL particles with both apoEC-J and apoEC-WT using a cholate dialysis method. Figure 6, upper panels, shows the electron microscopic images of these recombinant HDL particles. Measurements indicated that both particles using apoEC-J and apoEC-WT display a diameter of 21−22 Å on average with an equal size distribution. These data suggest that both apoEC-J and apoEC-WT have an equal ability of making recombinant HDL particles with similar diameters. In conclusion, the apoEC-J mutant is a monomeric, biologically active apoE C-terminal domain.

NMR Study of Monomeric, Biologically Active ApoEC-J. CD studies indicate that apoEC-J adopts an α-helical structure with a helical content of ∼40% in 100 mM phosphate buffer without TFE or DPC micelles. However, in a helix-stabilizing solvent, such as trifluoroethanol (TFE), or a lipid environment, such as dodecylphosphocholine (DPC), apoEC-J maintains its α-helical structure with a much higher helical content (84% in 30% TFE, 77% in 150 mM DPC) (Figure 7). To search for an experimental condition in which the NMR structural determination can be carried out, apoEC-J was doubly labeled with ^{15}N and ^{13}C, and NMR experiments were carried out under different sample conditions. Our results suggest that although apoEC-J adopts an α-helical structure in aqueous buffer, such as 100 mM phosphate buffer, this α-helical structure is very flexible. For

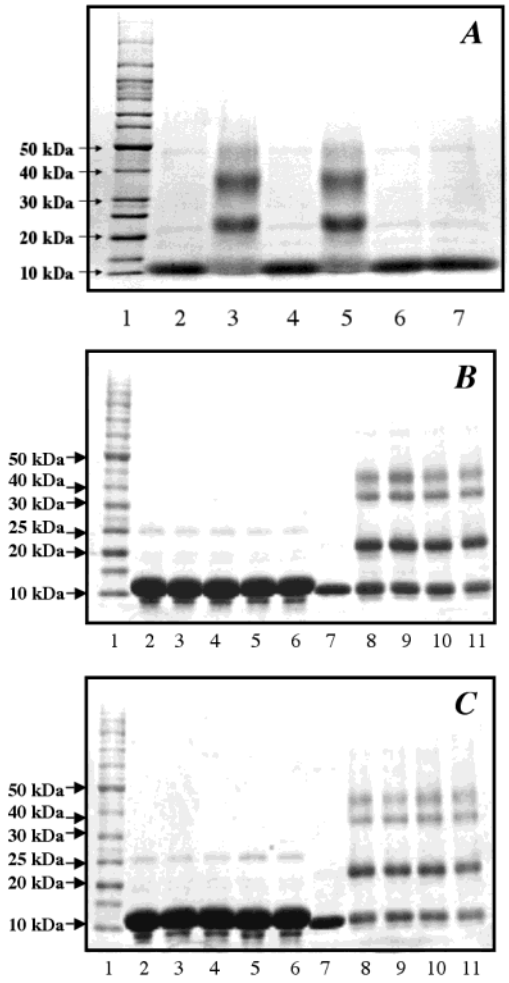

FIGURE 3: Panel A: 6−15% SDS−PAGE of apoEC-WT, apoEC-W264R, and apoEC-J with and without cross-linking under 20 mM phosphate buffer, pH 7.5. Lanes: 1, bench marker; 2, apoEC-WT without cross-linking; 3, apoEC-WT with cross-linking; 4, apoEC-W264R without cross-linking; 5, apoEC-W264R with cross-linking; 6, apoEC-J without cross-linking; 7, apoEC-J with cross-linking. All samples are at a protein concentration of 1−2 mg/mL. Panel B: 6−15% SDS−PAGE of cross-linking results of apoEC-WT (1 mg/mL) and apoEC-J (5 mg/mL) under 20 mM phosphate buffer at different pHs. Lanes: 1, bench marker; 2, apoEC-J non-cross-linked, pH 7.5; 3−6, apoEC-J cross-linked at pH 6.5, 7.0, 8.0, and 9.0; 7, apoEC-WT, non-cross-linked, pH 7.5; 8−11, apoEC-WT, cross-linked at pH 6.5, 7.0, 8.0, and 9.0. Panel C: 6−15% SDS−PAGE of cross-linking results of apoEC-WT (1 mg/mL) and apoEC-J (5 mg/mL) under 20 mM phosphate buffer, pH 7.5, and different NaCl concentrations. Lanes: 1, bench marker; 2, apoEC-J non-cross-linked, pH 7.5, 0 mM NaCl; 3−6, apoEC-J cross-linked at 0, 100, 200, and 300 mM NaCl, pH 7.5; 7, apoEC-WT, non-cross-linked, pH 7.5, 0 mM NaCl; 8−11, apoEC-WT cross-linked at 0, 100, 200, and 300 mM NaCl, pH 7.5.

example, a 2D NOESY spectrum of apoEC-J at 30 °C displays a small number of cross-peaks but significantly more cross-peaks at 10 °C with the same sample (data not shown). On the other hand, apoEC-J adopts a well-defined helical structure either in 30% TFE or in the presence of DPC at 30 °C. Importantly, cross-linking results indicated that apoEC-J was monomeric in 30% TFE, pH 5.7, at 10 mg/mL, whereas apoEC-WT displayed predominantly monomer (∼55%) and dimer (∼40%) with minor higher oligomers (∼5%) under the same condition (data not shown). Figure 8 shows $^{15}N-^{1}H$ HSQC NMR spectra of apoEC-J in 200 mM phosphate buffer, pH 5.7, with 5% D_2O and 30% TFE at 30 °C (panel

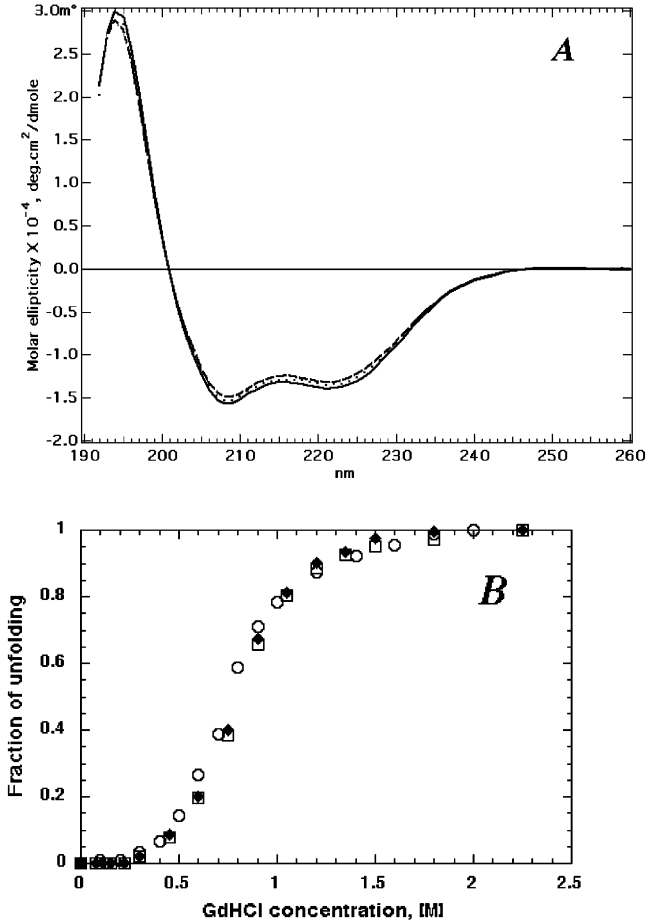

FIGURE 4: Panel A: Far-UV CD spectra of apoEC-WT, apoEC-W264R, and apoEC-J in 50 mM phosphate buffer, pH 7.0, at 0.1 mg/mL. Solid black line, apoEC-WT; dotted line, apoEC-W264R; broken line, apoEC-J. Panel B: Guanidine hydrochloride denaturation of apoEC-WT (□), apoEC-W264R (◆), and apoEC-J (○). The fraction of unfolding was plotted as a function of guanidine hydrochloride concentration.

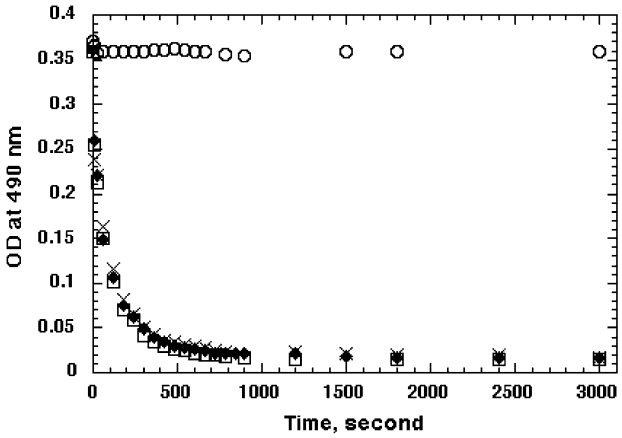

FIGURE 5: Phospholipid vesicle clearance. DMPC vesicles were incubated at 24 °C in the absence (○) and presence of apoEC-WT (□), apoEC-W264R (◆), and apoEC-J (×) in 20 mM Tris-HCl, pH 7.2, 250 mM NaCl, and 1 mM EDTA. Vesicle clearance as a function of time was followed by OD at 490 nm.

A) and in 200 mM phosphate buffer, pH 5.7, with 5% D_2O and 150 mM DPC at 30 °C (panel B). As expected for a helical protein, the cross-peaks are generally upfield shifted with less chemical shift dispersion. This is confirmed by the chemical shift of the α-protons (∼3.5−4.5 ppm) using a 2D

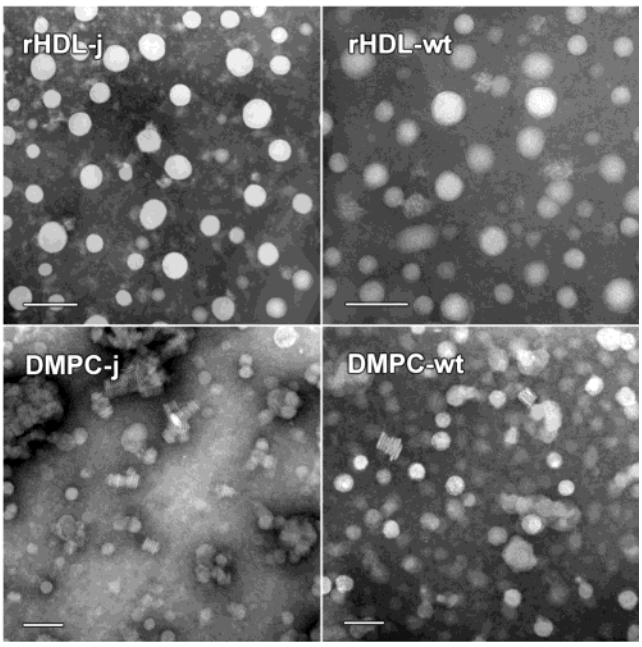

FIGURE 6: Electron micrographs of rHDL and DMPC particles with apoEC-WT or apoEC-J. Samples were negatively stained with 2% phosphotungstic acid. Bar = 40 nm (rHDL-j, rHDL-wt, DMPC-wt) or 50 nm (DMPC-j). The average diameters and the standard deviations of the particles are the following: rHDL-j, 21.0 ± 4.3 nm; rHDL-wt, 22.2 ± 4.6 nm; DMPC-j, 18.1 ± 3.3 nm; DMPC-wt, 18.5 ± 4.0 nm. These measurements are based on the particles with a diameter peak <30 nm.

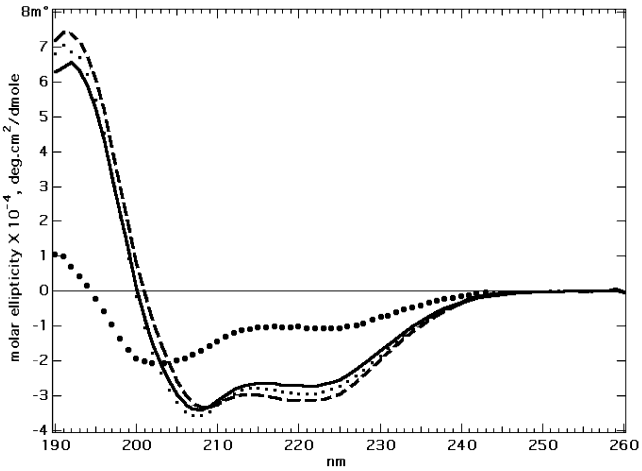

FIGURE 7: Far-UV CD spectra of apoEC-J in 30% TFE (broken line), 100 mM DPC (solid line), 100 mM SDS (light dotted line), and 100 mM phosphate buffer (heavy dotted line). All samples are in 100 mM phosphate buffer, pH 5.4, at a concentration of 0.1 mg/mL.

NOESY spectrum (data not shown). The chemical shift dispersion in both of the HSQC spectra is ~2.0 ppm in the HN dimension and ~22 ppm in the ^{15}N dimension, indicating that apoEC-J may adopt a helical-bundle-like structure. Overall, Figure 8 demonstrates that apoEC-J displays high-quality NMR spectra that can be used to generate NMR structures of this protein in both the lipid-free and lipid-bound states.

DISCUSSION

The X-ray crystal structure of the apoE N-terminal domain, reported in 1991, provided the first high-resolution structure of apoE, which significantly enhanced our understanding of the structure−function relationship of this protein (*13*). However, no further structural information about the apoE C-terminal domain or full-length apoE has been reported since then. In 1999, a diffraction-quality crystal of residues 223−272 of the apoE fragment was reported (*12*); however, no structural determination of this crystal has been reported. The aggregation property and intrinsic flexibility of the apoE C-terminal domain hinder NMR studies of this protein and prevent it from crystallization. To circumvent these problems, we prepared a monomeric, biologically active apoE C-terminal domain. We first developed a high-level expression system for the apoE C-terminal domain, allowing for routine production of 50 mg/L purified protein. Sequence alignment indicated that residues 253−289 form the most conserved region of the apoE C-terminal domain. Interestingly, this region is also the region that was previously reported as the region that causes apoE aggregation (*17*, *22*). Careful inspections of this region identified several consecutive bulky hydrophobic residues which are not observed in any other regions of apoE. These consecutive bulky hydrophobic residues are hypothesized to be responsible for apoE's aggregation, since they potentially form hydrophobic cross sections (Figure 2). Such hydrophobic cross sections are not stable in solution and are likely to aggregate to form oligomers. Our rationale is to mutate these consecutive bulky hydrophobic residues by either smaller hydrophobic residues or hydrophilic residues, thus reducing the size of the hydrophobic surface. This will disrupt the large hydrophobic cross sections, potentially breaking up the oligomerization of the apoE C-terminal domain. Thus, a monomeric apoE C-terminal domain may be generated.

On the basis of this rationale, a series of mutants of the apoE C-terminal domain was designed and prepared. Special attention was placed on the following residues, F257, W264, L268, V269, W276, L279, V280, and V287, since these residues are consecutive bulky hydrophobic residues (Figure 1). In addition, a strategy was taken in the initial stage of this study, which concentrated on the aggregation state of each mutant, whereas the biophysical/structural properties and the biological activity of the mutants were "ignored" at this stage. Thus, once we prepared a mutant, we would quickly characterize the oligomeric property of this mutant using cross-linking experiments. The cross-linking experiment is critical to this strategy since it provides us with a technique to quickly access the oligomeric state of each mutant at an NMR sample concentration. If this mutant were not a monomer, we would quickly design a new mutant. This procedure was repeated until a complete monomer at an NMR concentration was finally obtained. Using this strategy, a monomeric mutant, apoEC-J, was quickly identified.

A thorough study of this monomeric mutant, apoEC-J, was carried out to characterize its biophysical/structural properties and biological activity. In this case, the wild-type protein, apoEC-WT, and a single site mutant, apoEC-W264R, were used as the control. Our results demonstrated that the generated monomeric apoE C-terminal mutant, apoEC-J, adopted a secondary structure and thermodynamic stability identical to that of the wild-type protein, monitored by CD spectroscopy and denaturation experiments using GdnHCl. This suggests that residues F257, W264, V269, L279, and V287 may not be critical in maintaining the α-helix structure

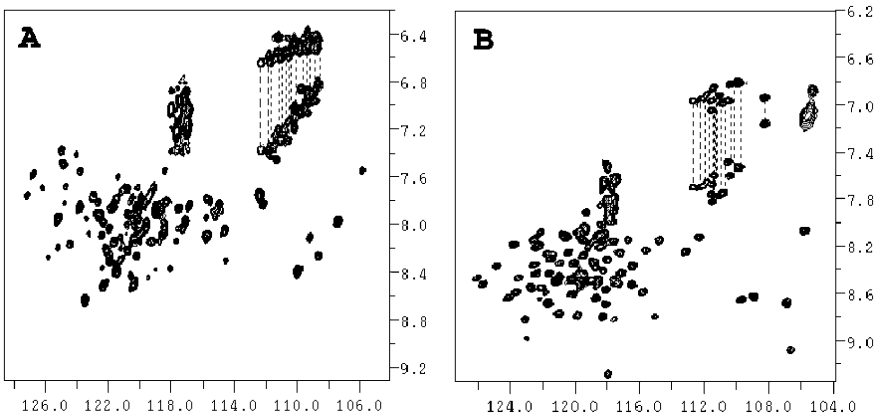

FIGURE 8: Two-dimensional $^1H-^{15}N$ heteronuclear single-quantum correlation spectra of uniformly ^{15}N-labeled apoEC-J in 200 mM phosphate buffer, pH 5.7 at 30 °C. Panel A: in the presence of 30% TFE-d_3, 65% H_2O, and 5% D_2O. Panel B: in the presence of 150 mM DPC-d_{38}, 95% H_2O, and 5% D_2O.

and stability of the apoE C-terminal domain. Thus, an NMR structure of apoEC-J should represent the solution structure of this apoE domain. A preliminary NMR structural study of apoEC-J was carried out and found that it is very flexible in buffers, even though it adopts an α-helical structure. However, in the presence of either TFE or DPC, the α-helical structure of apoEC-J is significantly stabilized. TFE is known to stabilize or, in some cases, promote a native-like helical structure in proteins and, thus, is widely used as a cosolvent for helical proteins (*31*, *32*). However, in several other cases, TFE was shown to promote the formation of non-native structures in proteins (*33*, *34*). In our case, the CD data indicated that the apoEC-J mutant itself adopted a flexible α-helical structure in solution, and TFE maintains and significantly stabilizes this native helical structure. In addition, apoEC-J in 30% TFE produced high-quality NMR spectra that can be used for the structural determination of this protein. The fact that apoEC-J displays a helical structure in aqueous buffer suggests that the α-helical structure in the presence of 30% TFE is not a structural artifact induced by TFE as a cosolvent, rather it represents a native structure of this protein in solution. On the other hand, DPC is a micelle-forming detergent that possesses a phosphocholine headgroup and a single C_{12} hydrocarbon chain. About 56 DPC molecules form a micelle (*35*). It has been reported that DPC micelles represent a good mimic of a monolayer lipoprotein surface (*36*). It is believed that the structure of apoEC-J in the presence of DPC micelles represents a lipid-bound structure of this protein. The NMR spectrum shown in Figure 8, panel B, of apoEC-J is in the presence of 150 mM DPC, which is >100-fold higher concentration than the critical micelle concentration (CMC) of DPC (1.1 mM). Thus, the DPC micelle concentration is about 2.6 mM which is >2-fold of the apoEC-J concentration (~1.0 mM). Under this experimental condition, it is anticipated that only one apoEC-J molecule binds to one micelle. In such a lipid surface mimetic environment, apoEC-J once again adopted a helical structure (Figure 7). However, the NMR spectra shown in Figure 8 indicated a significant spectral difference between apoEC-J in the presence of 30%TFE and that in the presence of DPC micelles, suggesting that apoEC-J may adopt different α-helical structures between the lipid-free and lipid-associated states. The cross-peaks observed in the $^{15}N-^1H$ HSQC spectra correlate the chemical shift of amide protons with ^{15}N-labeled amide nitrogen of the same amino acid. Thus, each cross-peak represents one amino acid, except the pairs of cross-peaks in the upper right corner, connected by dotted lines, which represent the side-chain NH_2 of Asn and Gln. The NMR structural determination of apoEC-J in these two different environments should provide both the lipid-free and lipid-bound structures, permitting us to elucidate the conformational changes of the apoE C-terminal domain upon lipid binding. Indeed, Figure 8 demonstrates that high-quality NMR spectra of apoEC-J are collected under both 30% TFE and DPC conditions, allowing for a complete NMR spectral assignment and structural determination of this protein in both lipid-free and lipid-bound states.

To access the lipid-binding activity, the apoEC-J mutant was first evaluated using a DMPC-binding assay. The DMPC vesicle was prepared (~200 nm in diameter) and showed a turbid appearance, which, at 24 °C, rapidly cleared upon the addition of apoEC-WT. This is because apoEC-WT binds to DMPC vesicles to transform larger DMPC vesicles into a much smaller discoidal apoEC-WT/DMPC complex, which is transparent. This spontaneous clearance can be monitored by right-angle light scattering spectroscopy or visible light absorbance using a spectrophotometer. This DMPC-binding assay is widely used to characterize the lipid-binding activity of exchangeable apolipoproteins (*24*). Using this assay, we examined both apoEC-WT and apoEC-J. The data showed that apoEC-J displayed a vesicle clearance curve identical to that of apoEC-WT, including both the initial rate and the $t_{1/2}$ of DMPC vesicle clearance. This demonstrates that apoEC-J has an equal ability, as that of apoEC-WT, of transforming DMPC vesicles into disks, suggesting that apoEC-J is biologically active. To further confirm this conclusion, both apoEC-J and apoEC-WT were used to prepare rHDL particles. These prepared rHDL particles were characterized using native gel and electron microscopy. The results demonstrated that both apoEC-J and apoEC-WT formed recombinant HDL particles with similar particle sizes and shape, confirming the conclusion obtained using the DMPC clearance assay. With these two different lipid-binding assays, we are confident that apoEC-J is a monomeric, biologically active apoE C-terminal domain.

Weisgraber's group previously used several C-terminal truncation mutants, apoE(1−223), apoE(1−244), apoE(1−266), and apoE(1−272), to study apoE lipoprotein binding and tetramer formation with apoE(1−299) and apoE(1−191) as controls. Their results indicated that residues 268−289

are responsible for apoE's aggregation, whereas residues 225−272 are critical for lipoprotein binding (*17*, *22*). Consistent with these results, our data identified five residues, F257, W264, V269, L279, and V287, that are critical to the aggregation property of the apoE C-terminal domain. Importantly, mutations in these positions also maintain secondary structure/stability and the lipid-binding activity of this protein, suggesting that the aggregation property of the apoE C-terminal domain is independent from both the secondary structure/stability and lipid-binding activity of this protein. In other words, the lipid-binding activity of the apoE C-terminal domain does not require protein aggregation. This is consistent with previously published data, indicating that apoE does not appear to self-associate on lipid surfaces (*37*). Our results further indicate that the critical residues responsible for α-helical structure/stability and lipid-binding activity are different from the above five residues that are crucial for apoE's aggregation. Thus, it seems that the apoE C-terminal domain uses different sets of epitopes to regulate its lipid-binding activity, to maintain and stabilize its α-helical structure, and to mediate its aggregation. This conclusion should provide a structural/functional basis for the generation of a monomeric, biologically active, full-length apoE for structural determination of this important protein, and we are currently working on this project.

Taken together, our results conclude that a monomeric, biologically active apoE C-terminal domain, apoEC-J, has been successfully prepared. Using this mutant, it has been demonstrated that high-quality NMR spectra have been collected in both the lipid-free and lipid-bound environments, allowing for NMR structure determinations of the apoE C-terminal domain in the lipid-free and lipid-bound states. It is worth noting that such structures of the apoE C-terminal domain are currently not available. In addition, the success of preparing a monomeric, biologically active apoE C-terminal domain indicates that it is also possible to prepare a monomeric, biologically active, full-length apoE for an NMR structural determination. Furthermore, crystallization of such a monomeric, full-length apoE may also be possible. Therefore, this study has solved the major technical problem of aggregation in the structural studies of apoE and the apoE C-terminal domain.

ACKNOWLEDGMENT

The authors thank Daniel Leek, Robin S. Dothager, and Jianglei Chen for their help in protein expression and purification. The authors also thank Dr. Sheeja Vasudevan for critical reading of the manuscript and helpful discussion.

REFERENCES

1. Weisgraber, K. H. (1994) Apolipoprotein E: structure−function relationships, *Adv. Protein Chem. 45*, 249−299.
2. Mahley, R. W. (1988) Apolipoprotein E: cholesterol transport protein with expanding role in cell biology, *Science 240*, 622−630.
3. Zannis, V. I., Breslow, J. L., Utermann, G., Mahley, R. W., Weisgraber, K. H., et al. (1982) Proposed nomenclature of apoE isoproteins, apoE genotypes, and phenotypes, *J. Lipid Res. 23*, 911−914.
4. Rall, S. C., Jr., Weisgraber, K. H., and Mahley, R. W. (1982) Human apolipoprotein E. The complete amino acid sequence, *J. Biol. Chem. 257*, 4171−4178.
5. Schneider, W. J., Kovanen, P. T., Brown, M. S., Goldstein, J. L., Utermann, G., Weber, W., Havel, R. J., Kotite, L., Kane, J. P., Innerarity, T. L., and Mahley, R. W. (1981) Familial dysbetalipoproteinemia. Abnormal binding of mutant apoprotein E to low density lipoprotein receptors of human fibroblasts and membranes from liver and adrenal of rats, rabbits, and cows, *J. Clin. Invest. 68*, 1075−1085.
6. Stengård, J. H., Zerba, K. E., Pekkanen, J., Ehnholm, C., Nissinen, A., and Sing, C. F. (1995) Apolipoprotein E polymorphism predicts death from coronary heart disease in a longitudinal study of elderly Finnish men, *Circulation 91*, 265−269.
7. Weisgraber, K. H., and Mahley, R. W. (1996) Human apolipoprotein E: the Alzheimer's disease connection, *FASEB J. 10*, 1485−1494.
8. Wetterau, J. R., Aggerbeck, L. P., Rall, S. C., Jr., and Weisgraber, K. H. (1988) Human apolipoprotein E3 in aqueous solution. I. Evidence for two structural domains, *J. Biol. Chem. 263*, 6240−6248.
9. Aggerbeck, L. P., Wetterau, J. R., Weisgraber, K. H., Wu, C. S., and Lindgren, F. T. (1988) Human apolipoprotein E3 in aqueous solution. II. Properties of the amino- and carboxyl-terminal domains, *J. Biol. Chem. 263*, 6249−6258.
10. Strittmatter, W. J., Weisgraber, K. H., Huang, D. Y., Dong, L.-M., Salvesen, G. S., Pericak-Vance, M., Schmechel, D., Saunders, A. M., Goldgaber, D., and Roses, A. D. (1993) Binding of human apolipoprotein E to synthetic amyloid beta peptide: isoform-specific effects and implications for late-onset Alzheimer disease, *Proc. Natl. Acad. Sci. U.S.A. 90*, 8098−8102.
11. Golabek, A. A., Kida, E., Walus, M., Perez, C., Wisniewski, T., and Soto, C. (2000) Sodium dodecyl sulfate-resistant complexes of Alzheimer's amyloid beta-peptide with the N-terminal, receptor binding domain of apolipoprotein E, *Biophys. J. 79*, 1008−1015.
12. Forstner, M., Peters-Libeu, C., Contreras-Forrest, E., Newhouse, Y., Knapp, M., Rupp, B., and Weisgraber, K. H. (1999) Carboxyl-terminal domain of human apolipoprotein E: expression, purification, and crystallization, *Protein Expression Purif. 17*, 267−272.
13. Wilson, C., Wardell, M. R., Weisgraber, K. H., Mahley, R. W., and Agard, D. A. (1991) Three-dimensional structure of the LDL receptor-binding domain of human apolipoprotein E, *Science 252*, 1817−1822.
14. Innerarity, T. L., Pitas, R. E., and Mahley, R. W. (1979) Binding of arginine-rich (E) apoprotein after recombination with phospholipid vesicles to the low density lipoprotein receptors of fibroblasts, *J. Biol. Chem. 254*, 4186−4190.
15. Weisgraber, K. H., Lund-Katz, S., and Phillips, M. C. (1992) in *High Density Lipoproteins and Atherosclerosis III* (Miller, N. E., and Tall, A. R., Eds.) pp 175−181, Excerpta Medica, Hillsborough, NJ.
16. Weisgraber, K. H., Mahley, R. W., Kowal, R. C., Herz, J., Goldstein, J. L., and Brown, M. S. (1990) Apolipoprotein C-I modulates the interaction of apolipoprotein E with beta-migrating very low density lipoproteins (beta-VLDL) and inhibits binding of beta-VLDL to low density lipoprotein receptor-related protein, *J. Biol. Chem. 265*, 22453−22459.
17. Dong, L.-M., Wilson, C., Wardell, M. R., Simmons, T., Mahley, R. W., Weisgraber, K. H., and Agard, D. A. (1994) Human apolipoprotein E. Role of arginine 61 in mediating the lipoprotein preferences of the E3 and E4 isoforms, *J. Biol. Chem. 269*, 22358−22365.
18. Dong, L.-M., Parkin, S., Trakhanov, S. D., Rupp, B., Simmons, T., Arnold, K. S., Newhouse, Y. M., Innerarity, T. L., and Weisgraber, K. H. (1996) Novel mechanism for defective receptor binding of apolipoprotein E2 in type III hyperlipoproteinemia, *Nat. Struct. Biol. 3*, 718−722.
19. Dong, L.-M., and Weisgraber, K. H. (1996) Human apolipoprotein E4 domain interaction. Arginine 61 and glutamic acid 255 interact to direct the preference for very low density lipoproteins, *J. Biol. Chem. 271*, 19053−19057.
20. Maeda, H., Nakamura, H., Kobori, S., Okada, M., Mori, H., Niki, H., Ogura, T., and Hiraga, S. (1989) Identification of human apolipoprotein E variant gene: apolipoprotein E7 (Glu244, 245Lys244,245), *J. Biochem. (Tokyo) 105*, 51−54.
21. Tajima, S., Yamamura, T., Menju, M., and Yamamoto, A. (1989) Analysis of apolipoprotein E7 (apolipoprotein E-Suita) gene from a patient with hyperlipoproteinemia, *J. Biochem. (Tokyo) 105*, 249−253.
22. Westerlund, J. A., and Weisgraber, K. H. (1993) Discrete carboxyl-terminal segments of apolipoprotein E mediate lipoprotein association and protein oligomerization, *J. Biol. Chem. 268*, 15745−15750.

23. MacDonald, R. C., MacDonald, R. I., Menco, B. Ph. M., Takeshita, K., Subbarao, N. K., and Hu, L. (1991) Small-volume extrusion apparatus for preparation of large, unilamellar vesicles, *Biochim. Biophys. Acta 1061*, 297−303.
24. Surewicz, W., Epand, R. M., Pownall, H. J., and Hiu, S.-K. (1986) Human apolipoprotein A-I forms thermally stable complexes with anionic but not with zwitterionic phospholipids, *J. Biol. Chem. 261*, 16191−16197.
25. Jonas, A. (1986) Reconstitution of high-density lipoproteins, *Methods Enzymol. 128*, 553−582.
26. Jonas, A., Kezdy, K. E., and Wald, J. H. (1989) Defined apolipoprotein A-I conformations in reconstituted high density lipoprotein discs, *J. Biol. Chem. 264*, 4818−4824.
27. Pace, C. N., Shirley, B. A., and Thomson, J. A. (1989) in *Protein Structure and Function: a practical approach* (Creighton, T. E., Ed.) LRL Press, Oxford.
28. Delaglio, F., Grzesiek, S., Vuister, G. W., Zhu, G., Pfeifer, J., and Bax, A. (1995) NMRPipe: a multidimensional spectral processing system based on UNIX pipes, *J. Biomol. NMR 6*, 277−293.
29. Garrett, D. S., Powers, R., Gronenborn, A. M., and Clore, G. M. (1991) Methods to study membrane protein structure in solution, *J. Magn. Reson. 95*, 214−220.
30. Segrest, J. P., Garber, D. W., Brouillette, C. G., Harvey, S. C., and Anantharamaiah, G. M. (1994) The amphipathic alpha helix: a multifunctional structural motif in plasma apolipoproteins, *Adv. Protein Chem. 45*, 303−369.
31. Luo, P., and Baldwin, R. L. (1997) Mechanism of helix induction by trifluoroethanol: a framework for extrapolating the helix-forming properties of peptides from trifluoroethanol/water mixtures back to water, *Biochemistry 36*, 8413−8421.
32. Buck, M., Schwalbe, H., and Dobson, C. M. (1996) Main-chain dynamics of a partially folded protein: ^{15}N NMR relaxation measurements of hen egg white lysozyme denatured in trifluoroethanol, *J. Mol. Biol. 257*, 669−683.
33. Sonnichsen, F. D., Van Eyk, J. E., Hodges, R. S., and Sykes, B. D. (1992) Effect of trifluoroethanol on protein secondary structure: an NMR and CD study using a synthetic actin peptide, *Biochemistry 31*, 8790−8798.
34. Fan, P., Bracken, C., and Baum, J. (1993) Structural characterization of monellin in the alcohol-denatured state by NMR: evidence for beta-sheet to alpha-helix conversion, *Biochemistry 32*, 1573−1582.
35. Henry, G. D., and Sykes, B. D. (1994) Methods to study membrane protein structure in solution, *Methods Enzymol. 239*, 515−535.
36. Kallick, D. A., Tessmer, M. R., Watts, C. R., and Li, C.-Y. (1995) The use of dodecylphosphocholine micelles in solution NMR, *J. Magn. Reson. 109*, 60−65.
37. Yokoyama, S. (1990) Self-associated tetramer of human apolipoprotein E does not lead to its accumulation on a lipid particle, *Biochim. Biophys. Acta 1047*, 99−101.

BI035958W